Environmental Science
Atmospheres

ROYAL SOCIETY
OF CHEMISTRY

PAPER
Andrew P. Grieshop *et al.*
Development of volatility distributions for organic
matter in biomass burning emissions

Check for updates

Development of volatility distributions for organic matter in biomass burning emissions†

Aditya Sinha,[a] Ingrid George,[b] Amara Holder,[b] William Preston,[c] Michael Hays [ID] [b] and Andrew P. Grieshop [ID] *[a]

The volatility distribution of organic emissions from biomass burning and other combustion sources can determine their atmospheric evolution due to partitioning/aging. The gap between measurements and models predicting secondary organic aerosol has been partially attributed to the absence of semi- and intermediate volatility organic compounds (S/I-VOC) in models and measurements. However, S/I-VOCs emitted from these sources and typically quantified using the volatility basis framework (VBS) are not well understood. For example, the amount and composition of S/I-VOCs and their variability across different biomass burning sources such as residential woodstoves, open field burns, and laboratory simulated open burning are uncertain. To address this, a novel filter-in-tube sorbent tube sampling method collected S/I-VOC samples from biomass burning experiments for a range of fuels and combustion conditions. Filter-in-tube samples were analyzed using thermal desorption-gas chromatography-mass spectrometry (TD/GC/MS) for compounds across a wide range of volatilities (saturation concentrations; $-2 \leq \log C^* \leq 6$). The S/I-VOC measurements were used to calculate volatility distributions for each emission source. The distributions were broadly consistent across the sources with IVOCs accounting for 75–90% of the total captured organic matter, while SVOCs and LVOCs were responsible for 6–13% and 1–12%, respectively. The distributions and predicted partitioning were generally consistent with the literature. Particulate matter emission factors spanned two orders of magnitude across the sources. This work highlights the potential of inferring gas–particle partitioning behavior of biomass burning emissions using filter-in-tube sorbent samples analyzed offline. This simplifies both sampling and analysis of S/I-VOCs for studies focused on capturing the full range of organics emitted.

Environmental significance

Organic emissions from biomass burning are a key contributor to atmospheric composition at all scales. Organic volatility dictates their gas–particle partitioning and contribution to secondary organic aerosol formation. Previous studies have not addressed the volatility of the diverse range of biomass combustion types, largely due to the complexity of quantifying organic volatility. Here, we present results from a novel sampling and analytical approach applied to a range of biomass combustion systems (lab burning of wildland fuels, open grassland burning, residential wood combustion). Our results demonstrate that this relatively simple and field-deployable approach yields volatility distribution that are broadly consistent with previous estimates, but that are distinct between combustion types. While organic PM emission factors ranged over two orders of magnitude across the sources tested, volatility distributions had smaller, though consistent inter-source differences.

1. Introduction

Emissions from biomass burning significantly influence gas and particle concentrations globally.[1] These emissions include major greenhouse gases like carbon dioxide (CO_2), air pollutants like carbon monoxide (CO), and volatile organic compounds (VOCs) capable of undergoing photo-oxidation to form secondary products. The products of incomplete combustion from these emissions also include fine particles or particulate matter smaller than 2.5 μm ($PM_{2.5}$). $PM_{2.5}$ is an important atmospheric pollutant that has large yet uncertain impacts on climate,[1] air quality[2] and adversely affects human health.[3,4] Modeling studies have shown that residential emissions can make substantial contributions to ambient air pollution (*e.g.* ∼20−50% of $PM_{2.5}$ in India).[5,6] Further, emission inventories have estimated that 26−73% of global emission of fine particulate organic matter can be ascribed to open biomass burning and about 20% to residential biomass combustion.[7–10]

[a]Department of Civil and Environmental Engineering, North Carolina State University, Raleigh, NC, USA. E-mail: apgriesh@ncsu.edu

[b]Center for Environmental Measurement and Modeling, US Environmental Protection Agency, Durham, NC, USA

[c]CSS Inc., Durham, NC, USA

† Electronic supplementary information (ESI) available. See DOI: https://doi.org/10.1039/d2ea00080f

© 2023 The Author(s). Published by the Royal Society of Chemistry

Environ. Sci.: Atmos., 2023, **3**, 11–23 | **11**

This indicates that primary organic aerosol (POA) emitted from biomass burning forms an important component of $PM_{2.5}$. It is now well understood that biomass burning POA is semi-volatile in nature, *i.e.*, the organic compounds that constitute POA can partition between the gas and particle phases.[11–14] This partitioning can vary with atmospheric dilution and ambient temperature, which shift the thermodynamic equilibrium, influencing the fate and lifetime of biomass burning POA. Accounting for gas–particle partitioning in emissions inventories can have important implications for predictions of chemical transport models (CTMs) and enable more accurate depictions of atmospheric aerosols. Gas–particle partitioning also creates inconsistencies in the definitions of particulate organic matter between regulatory measurements and air quality research models/measurements.[15,16] However, few studies have made attempts to constrain the partitioning behavior of biomass burning POA.

The gas–particle partitioning of POA in the atmosphere is typically described using absorptive partitioning theory.[17,18] This theory can be used in a semi-empirical fashion with a set of surrogate or lumped species that describes the measured partitioning behavior of emissions.[12,14] This surrogate set of compounds is often represented using a one-dimensional volatility basis set, or VBS,[18] which distributes organics over a logarithmically spaced set of bins of effective saturation concentration, C_i^*. In this framework, resolution of POA at a molecular level is not required as surrogate bins describe the properties of compounds lumped in the bin (*e.g.*, saturation concentration). At phase equilibrium, the organic aerosol (OA) emission factor (EF_{OA}) and the mass fraction of organic emissions residing in the particle phase (X_p) are expressed as:

$$X_p = \sum f_i \left(1 + \frac{C_i^*(T)}{C_{OA}} \right)^{-1} = \frac{EF_{OA}}{EF_{TOT}} \qquad (1)$$

where $C_i^*(T)$ is the effective saturation concentration of species i at temperature T, C_{OA} is the OA concentration, f_i is the mass fraction of species i, and EF_{TOT} is the emission factor of all lower-volatility organics (particle and gas phase) being captured.

Organics can be segregated into volatility groups based on the nomenclature proposed elsewhere[19,20] as: intermediate volatility organic compounds, IVOCs ($C^* = 300–3 \times 10^6$ µg m^{-3}), semi-volatile organic compounds, SVOCs ($C^* = 0.3–300$ µg m^{-3}) and low volatility organic compounds, LVOCs ($C^* < 0.3$ µg m^{-3}). S/I-VOCs play an important role in describing gas–particle partitioning from biomass burning emissions. S/I-VOCs are also important precursors for secondary organic aerosol (SOA) formation and likely play a key role in reducing the gap between measurements and models predicting SOA formation.[13,21] However, quantitative collection and chemical analysis of this material, and especially IVOCs, is complex. For example, in gas chromatography (GC) analysis, the vast majority of IVOCs typically elute in the chromatogram as unresolved complex mixtures (UCM), which is material that co-elutes and cannot be separated into individual compounds.[22,23] This is because IVOCs, typically consisting of compounds with carbon numbers greater than 10, are associated with a larger number of constitutional isomers, making them harder to resolve using traditional GC methods. As a result, little research has explored the speciation of S/I-VOCs in both gas and particle phases from biomass burning emissions. Previous studies have sampled from controlled/closed burning and reported gas and particle phase S/I-VOCs for three types of residential wood combustion (RWC)[24] and also measured RWC emissions with online methods.[25] Other studies have explored emissions from uncontrolled/open burning emissions. For example, one analysis explored emissions from six foliar fuels using ion chromatography and wavelength dispersive X-ray fluorescence techniques.[26] Another investigated emissions from a range of fuel types and burning conditions, including laboratory, fireplace, and prescribed fires using electron impact ionization gas chromatography interfaced with mass spectrometry.[27] A key commonality of these studies of speciated S/I-VOC compounds is that they typically only identify a fraction (40–50% or less) of the total mass with the remaining fraction apportioned to the UCM. Speciation methods thus have offered detailed chemical information on the identified fraction but have thus far not characterized the UCM (majority contribution in terms of mass). On the other hand, bulk methods (*e.g.*, thermooptical filter measurements of OC) offer little chemical detail but, depending on sampling media, are more likely to capture the full range of mass sampled. Thus, there exists a tradeoff in detailed speciation measurements and measuring the full volatility range of organic mass.

Several methods have been used to estimate volatility distributions of combustion emissions over the last decade. The positive artifact on quartz filters has been used to provide an estimate of gas–particle partitioning.[14,28–30] Isothermal dilution and temperature perturbations using thermodenuders have been used to constrain gas–particle partitioning of biomass burning aerosol from wood stoves[31] and laboratory fires.[11] Several studies have shown that equilibrium cannot be assumed when using thermal denuder systems, thus this tool typically requires application of kinetic equations to estimate volatility distributions.[32–34] More recently, a study has estimated volatility distributions of sewage incineration emissions using online mass spectroscopy, capable of measuring low concentrations of gas- and particle phase organics in real-time.[35] Another strategy has been the use of thermal desorption gas chromatography mass spectrometry (TD/GC/MS) to infer POA volatility *via* separation across the retention time in the GC column of organics desorbed from sorbent tubes.[22,30,36–39] The volatility distributions derived from TD/GC/MS measurements have been shown to be in agreement with distributions from isothermal dilution/temperature perturbations with kinetic modeling for diesel and gasoline engine emissions.[28,30] This method allows for the estimation of organic aerosol volatility from a single sample and thus offers an important advantage over more resource intensive online approaches (*e.g.*, thermodenuders, dilution). However, this method has not been previously used to characterize biomass burning POA volatility. Moreover, a variation of this method with the filter placed inside the sample collection tube allowing for sampling of gas and particle phase

organics for simultaneous analysis in the TD/GC/MS has not been attempted for biomass burning emissions. This novel filter-in-tube measurement approach would simplify both sampling and analysis of sorbents for studies focused on capturing the full range of S/I-VOCs emitted.

Biomass burning spans a spectrum ranging from residential wood stoves to open burning resulting in complex mixtures of organic compounds that span a wide range of volatility. Studies have constrained the volatility distributions of biomass burning POA emissions from wood stoves[12] and also from laboratory burns of 15 fuels over a range of combustion conditions.[11] The recommended distributions derived in May *et al.*[11] have been used in several modeling studies.[40–42] Other studies have obtained distributions for open-burning emissions *via* factor analysis of ambient and thermally denuded OA.[43] Another approach was to sample on Solid Phase Extraction (SPE) filters for untargeted analysis of gas-phase S/I-VOCs in biomass burning smoke samples from a series of laboratory fires and subsequently derive volatility distributions from the speciated data.[44] However, there is still uncertainty in the amount and composition of S/I-VOCs and how they are influenced by factors like fuel type and combustion conditions. Moreover, quantitative comparison of samples of fresh emissions from lab simulated open burning with those from real-world open burning is lacking. Thus, there is a need to measure partitioning parameters across a broader range of biomass burning conditions and compare them with existing parameterizations.

In this study, we address these knowledge gaps by measuring the volatility distributions from three different types of biomass burning emissions: open field burns, laboratory-simulated open burns and different phases of residential wood combustion in a modern heating stove. S/I-VOC volatility was investigated using a calibration built from *n*-alkane standards in TD/GC/MS analyses. The objectives of this study are as follows: (1) develop an approach and calibration to map TD/GC/MS data to VBS space; (2) characterize deviations from *n*-alkane-based calibration in deriving volatility distributions from TD/GC/MS chromatograms; (3) compare volatility distributions from different types of biomass burning using filter-in-tube sorbent samples analyzed using a TD/GC/MS; (4) make comparisons of the derived volatility distributions to existing distributions for biomass burning in literature.

2. Materials and methods

2.1 Experimental setup of combustion experiments

Several different sample types were collected to capture a range of biomass burning conditions, including in-field open burning, laboratory simulations of open burning, and laboratory testing of woodstoves. Sampling times and dilution ratios for the S/I-VOC samples were designed to obtain approximately the same amount of sample mass over the entire duration of each process, while avoiding breakthrough conditions. Breakthrough testing across several emissions testing environments was conducted, including those examining wildfire, residential burning, and vehicle emissions. Breakthrough testing is normally accomplished by positioning two tubes in series and

analyzing both using identical GC-MS methodology. At the flow rates, dilution ratios, and concentrations in the present study, compound breakthrough in the second tube has not been observed. In addition, the recovery of the internal standards spiked before sampling was monitored, and the d8-naphthalene internal standard recovery would indicate breakthrough issues during each sampling event.

In-field open burning (also referred to as 'field'): emissions were sampled from three in-field burns of Tallgrass Prairie in the Flint Hills region of Kansas in April 2019. Mobile measurement platforms were positioned immediately downwind of the burning field to capture fresh emissions (Fig. S1-A†). Background air samples were taken on days when no burning occurred. Concurrent measurements of CO, CO_2, $PM_{2.5}$, and elemental (EC) and organic carbon (OC) were made using a portable sampling package described elsewhere.[45,46] Briefly, continuous measurements of CO_2 were made with a nondispersive infrared analyzer (LiCor, Li-820) and CO with an electrochemical sensor (SGX, EC4-500). Batch samples with Teflon (Teflo, Pall) and quartz (Tissuquartz, Pall) 47 mm filters behind a $PM_{2.5}$ impactor inlet were taken simultaneously with a pressure-compensating pump at 10 l min^{-1} (Leland Legacy, SKC). EC and OC were quantified using the modified NIOSH 5040 protocol described elsewhere.[47]

Laboratory simulations of open burning (also referred to as 'burnhut'): fuel was collected from two locations in a conifer forest in northern and central Minnesota. The fuel samples consisted of four clip plots (two 1 m^2 and two 0.25 m^2) consisting of mostly moss and tree litter and two peat cores taken from the same sites. Open biomass burning was simulated in an open burn test facility (OBTF) on the EPA campus in Research Triangle Park, NC[48] (Fig. S1-B†). The OBTF is a 70 m^3 room with a high-volume blower that pulls ambient air into the room and out through an exhaust duct (12 inch diameter) to provide excess oxygen conditions. Fuels were dried at 80 °C overnight in an oven before burning. Fuels were evenly dispersed across a 0.5 m^2 stainless steel pan filled with sand and covered with aluminum foil and ignited with a propane torch. A nichrome wire was used to ignite the peat cores at one end resulting in smoldering combustion front propagating across the core. Emissions measurements were all taken in the exhaust duct at the same location. Batch samples for $PM_{2.5}$, EC, OC were collected through a 12 mm OD stainless-steel sample probe and $PM_{2.5}$ cyclone (URG). An aerosol splitter was used to split the sample between 47 mm Teflon filters (Teflo, Pall) and 90 mm quartz filters (Tissuquartz, Pall). S/I-VOC and black carbon samples were collected through a 6 mm OD stainless-steel sample probe. Continuous measurements of CO, CO_2 (CAI, 600 series), NO_x (EcoPhysics nCLD), and total hydrocarbons (THC) (CAI, 600 series) were collected through a 6 mm OD stainless-steel probe, heated filter, and heated Teflon sample line.

Laboratory testing of woodstoves (also referred to as 'RWC'): residential wood combustion (RWC) emissions were sampled from an EPA 2015 certified woodstove (Englander, 30-NC) following a modified cordwood test protocol (ASTM E3053). The method includes a startup phase followed by a high fire phase

© 2023 The Author(s). Published by the Royal Society of Chemistry

Environ. Sci.: Atmos., 2023, **3**, 11–23 | 13

Environmental Science: Atmospheres

Paper

where the stove air inlets are fully opened and ending with a low fire phase where stove air inlets are fully closed. Tests were done in triplicate for two fuel types: dry Red Oak and dry Sitka Spruce. Fuel wood was cut to nominally 40 cm in length and split into triangular pieces with the bark on (~0.5–2.5 kg). The test facility is described in detail elsewhere[49] and a schematic shown in Fig. S1-C.† Briefly, stove emissions are captured by a hood into an exhaust duct and subsequently mixed with filtered air to reduce temperatures and concentrations. Gas phase emissions (CO_2, CO, THC, NOx; CAI 600 series) were sampled through a stainless-steel probe, heated filter, and heated sample line from the dilution duct. $PM_{2.5}$ (47 mm Telfo, Pall) and EC/OC (47 mm Tissuquartz, Pall) samples were taken from the duct through 6 mm OD stainless steel probes. A secondary dilution system (DI-1000, Dekati) was used to further reduce pollutant concentrations so that SVOC samples could be collected over the entire test phase duration and have concentrations comparable to the field and burnhut samples. SVOC and black carbon (MA350, Aehtlabs) were sampled from a manifold connected to the secondary dilution system. Emissions were sampled from the exhaust duct with a stainless-steel probe (3/8″) using an eductor (DI-1000, Dekati) supplied with 20 l min⁻¹ of dilution air dried and scrubbed of CO_2 (Van Air Compressed Gas Dryer) and supplied to a stainless-steel (Schedule 40 2″ pipe) sampling manifold. The eductor provides a nominal 8 : 1 dilution ratio; but is dependent on the absolute pressure in the exhaust so the CO_2 concentration in the diluted air was measured continuously (LiCor, Li-820) to determine the dilution ratio. Background samples were taken from the dilution duct when the stove was not operating.

S/I-VOC emissions were sampled using filter-in-tube sorbents near the source or from the exhaust ducts (Fig. S1†). A flow of 0.07 l min⁻¹ through the sorbent tubes was maintained using a pump (Sensidyne Micro Air Diaphragm pump) and mass flow controller (Alicat, MC series). Actual sample flow was checked with a TSI flow calibrator before and after each sampling period. S/I-VOC sampling media consisted of 40 mm of Carbotrap-F (20/40 mesh) and 20 mm of Carbotrap-C (20/40 mesh) sorbents (purchased already filled in sorbent tubes by Sigma-Aldrich) with previously baked (550 °C for 8 hours) quartz filter punches (0.385 cm²) placed in the Gerstel tube upstream of the sorbent beds to capture both particle and gas phase emissions. This sorbent configuration was chosen as the measurement of hydrocarbons was a focus in our experiments, since they formed the basis of our volatility distribution estimation method (described in detail in Section 2.3). The sorbent tubes themselves were baked in a Gerstel TDS3 thermal desorption system to thermally clean them before packing. Prior to sampling and subsequent TD/GC/MS analysis, each tube was spiked with 1 microliter of a deuterated internal standard (Wisconsin State Lab of Hygiene Internal Standard #4, deuterated n-alkanes) to track analyte recovery. The internal standard solution contained six deuterated n-alkanes ranging from n-pentadecane-d32 ($C_{15}H_{32}$) to n-hexatriacontane-d74 ($C_{36}H_{74}$).

Sorbent tube samples with quartz fiber filter punches upstream of the sorbent material ("filter-in-tubes") were analyzed using a thermal desorption gas chromatography mass spectrometer (TD/GC/MS) (Gerstel TDS2, MD, USA) measuring total ion chromatograms (TIC), which we use to indicate the mass of gas- and particle-phase (i.e., total) S/I-VOCs sampled. During desorption, the TD was ramped from an initial temperature of 25 °C to a final hold temperature of 300 °C (7 min) at 60 °C s⁻¹. The Cooled Injection System (CIS) was held at an initial temperature of −100 °C during sample transfer. The GC was equipped with an Agilent HP-5 MS capillary column (30 m × 0.25 mm inner diameter). The GC method used a column flow of 1 mL min⁻¹. The initial GC oven temperature was fixed at 65 °C (held for 10 minutes) and ramped up to 300 °C at a rate of 10 °C min⁻¹ then held for 26.5 minutes. The MS was operated in scan mode to obtain total ion chromatograms reporting all measured signals. Other operational details regarding TD/GC/MS operation are furnished in Table S1.†

2.2 TD/GC/MS calibration experiments

In separate experiments, sorbent tubes were prepared with calibration spikes of n-alkanes, PAHs, sugars and methoxyphenols with constituents listed in Table S2.† Calibration spikes of 10 ng of each compound in the standard mixture were prepared by diluting with a HIB solvent solution (hexanes – 40%, isopropanol – 20%, benzene – 40% by volume). After the spike, nitrogen (N_2) was flowed through the tube at 50 mL min⁻¹ for 90 seconds to ensure proper transfer across the adsorbent material.

2.3 Chromatograph analysis

Before analyzing a sorbent tube collected from a biomass burning experiment, a calibration run using an n-alkane standard containing even alkanes ranging from C_{10}–C_{38} was first analyzed in scan mode. Fig. S2† depicts the subsequent steps involved in the derivation of volatility distributions from TICs of a biomass burning sample using the VBS framework. First, the TIC of the biomass burning sample was corrected for column bleed by deriving a correction factor, calculated as the ratio of the contribution of m/z 207 to the TIC signal in the chromatogram retention time window between 40 and 45 minutes, where column bleed dominates the signal. The column bleed corrected TIC was then divided into 29 bins in GC retention time space. The roughly equal width of the bins was dictated by GC retention times of n-alkanes ranging from C_{10}–C_{38}. The elution time of n-alkanes was used to define the volatility bin edges calculated as follows: if C_n represents the elution time of an n-alkane, the start point for the bin would be: $(C_n + C_{n-1})/2$ and the end point would be: $(C_n + C_{n+1})/2$. The only exceptions were the start of the C_{10} bin which was calculated as: $C_{10} - \left(\dfrac{C_{10} + C_{11}}{2} - C_{10}\right)$ and the end point of the C_{38} bin calculated as: $C_{38} + \left(C_{38} - \dfrac{C_{37} + C_{38}}{2}\right)$. An n-alkane series was chosen as the basis of this calibration for several reasons. First, since the GC column used a non-polar stationary phase, the retention times of aliphatic compounds corresponded to their boiling points and consequently, vapor pressures. Next, the saturation concentration of n-alkanes vary systematically

with carbon number.[36,50] It has also been shown that there is an approximately linear relationship between retention time and saturation concentration for hydrocarbons measured by the same analytical protocol.[36]

Next, the integrated areas within each GC retention time bin were calculated from the TIC. Each GC retention time was ascribed a carbon number bin based on the 29 n-alkane bins constructed during the previous step. The integrated bin areas are then calculated by summing within carbon number bins. A response factor, defined as the ratio of peak area to concentrations, was calculated for each sample using the deuterated n-alkane internal standard, and applied to the 29 integrated bin areas to convert them to bin masses. A minimum detection limit (MDL), defined as the bin area normalized to the corresponding internal standards, was determined from blank runs and applied as a threshold to each bin. This binning approach allowed us to calculate the mass fraction of total organics in each bin as the fraction of the integrated bleed-corrected TIC signal in each bin. In the final step, n-alkane carbon bins are mapped to saturation concentration (C^*) using a group contribution method, SIMPOL,[51] to represent volatility distributions in terms of the VBS framework.

Our approach assumes that the UCM, which dominates the TIC signal, behaves similar to n-alkane compounds used in our calibration. A similar approach has been used by another study, where m/z 57 was analyzed instead of the TIC.[36] The entire TIC signal has also been previously used for determination of volatility distributions from vehicle emissions.[37,38] This method captures the volatility distribution for all species which elute (in the UCM or otherwise) but cannot account for compounds which may not elute/only partially elute from the GC column (like some oxygenated compounds).

2.4 Data reduction

Emission factors. Fuel-based emission factor (EF) values were calculated for particle-phase pollutants (PM$_{2.5}$, OC, EC) using the carbon balance method described elsewhere,[52] to allow for comparison across different sources and fuels and enable comparisons to values in literature. EFs in units of g of pollutant kg^{-1} of fuel were calculated by:

$$\text{EF}_X = \frac{\Delta X}{(\Delta CO_2 + \Delta CO + \Delta THC)} \times \frac{1}{W_C} \times mf_C \qquad (2)$$

where ΔX is background corrected pollutant (g m^{-3}) and ΔCO_2, ΔCO, and ΔTHC are the background corrected CO_2, CO and total hydrocarbon (THC) concentrations (mol m^{-3}), respectively. W_C is the atomic weight of carbon (12 g mol^{-1}) and mf_C represents the mass fraction of carbon in biomass for which we assumed a value of 0.5, consistent with other work.[52] Total hydrocarbons were not measured in field combustion samples, so are not included in those calculations. However, THC contributes 3% of total emitted carbon for RWC tests, for which combustion conditions are most similar (Fig. 2), so we expect it has minor influence on calculated emission factors. Modified combustion efficiency (MCE) was calculated using background corrected CO_2 and CO values (MCE = $\Delta CO_2/(\Delta CO_2 + \Delta CO)$).

Volatility distributions. The final volatility distributions presented in Section 3.4 are obtained based on the following steps: (1) derive the bin masses as a function of C^* (in the range 10^{-2} µg m^{-3} $\leq C^* \leq 10^6$ µg m^{-3}) using the raw TIC as described in detail in Section 2.2 and divide by sample flow to calculate concentration in each bin; (2) correct the concentration in all bins with a correction factor, derived based on the ratio of the organic mass collected on quartz filters to the organic mass as estimated from the partitioning equation of the filter-in-tube TD/GC/MS samples (correction factor derivation is described in detail in Section S1†); (3) calculate volatility-bin-specific emission factors using the carbon balance method (eqn (2)); (4) normalize each C^* bin emission factor by the total emission factor to calculate the bin mass fraction (f_i).

3. Results and discussion

3.1 TD/GC/MS calibration with standard mixtures

To interpret the full scan TICs collected from biomass burning emission samples, calibration experiments described in Section 2.2 were conducted. Fig. 1A shows the resulting calibration for C^* as a function of GC elution time for a suite of standard compounds including straight chain alkanes, PAHs, methoxyphenols, levoglucosan and saturated acids. Within a compound series, more volatile compounds (higher C^*) elute earlier. The plot suggests that compounds in the PAH standard can be described by a similar C^* calibration curve as n-alkanes indicated by similar slopes, intercepts and R^2 values (log C^* = $-0.41 \times$ retention time + 13.6, R^2 = 0.97, fits not pictured in Fig. 1A). However, separate curves may be necessary for methoxyphenols and saturated acids. These differences may be driven at least partly by differences in polarity[53] that shift elution times for the alkanes/PAHs relative to the other classes of compounds explored here.

The vertical dashed lines in Fig. 1A show the boundaries of the C^* bins defined based on n-alkane retention times. The bins are defined such that compounds half a decade greater and lesser than the bin center in saturation concentration are included in a given bin. For example, the bin representing log C^* = 5 includes all compounds with $4.5 \leq \log C^* < 5.5$. Material eluting after 38 minutes in the chromatogram cannot be resolved further and is lumped with C^* = 10^{-2} µg m^{-3} bin, which will be in the condensed phase under essentially all atmospheric conditions. Quantifying emissions in bins up to $\log_{10} C^*$ = 6 captures S/I-VOCs, which likely represent a substantial fraction of SOA precursors.[12] Fig. 1A illustrates how compounds from the TIC (including UCM) can be ascribed to C^* bins based on the corresponding n-alkane eluting in that bin.

Fig. 1B shows response factors for different classes of compounds as a function of n-alkane carbon bins. As shown in Fig. 1A, the n-alkane carbon bin number of a compound is based on the GC retention time of the corresponding eluting n-alkane. In this way, methoxyphenols, PAHs and levoglucosan are presented on the same 'equivalent' n-alkane basis. The response factors were derived from calibration runs where known amounts of standard compounds are spiked onto
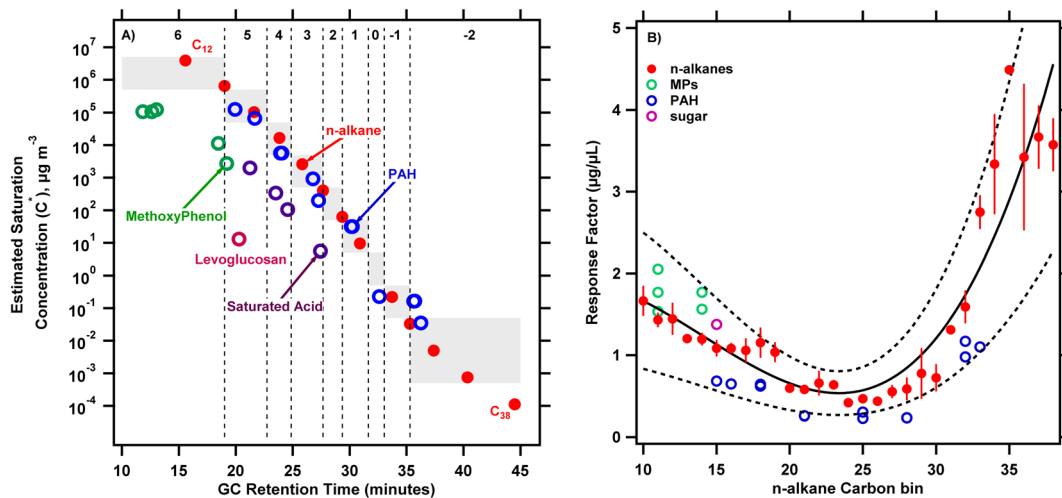
© 2023 The Author(s). Published by the Royal Society of Chemistry

Environ. Sci.: Atmos., 2023, **3**, 11–23 | 15

Fig. 1 (A) Estimated saturation concentration, C^*, plotted against GC retention time for calibration compounds – n-alkanes, PAHs, methoxyphenols, saturated acids and levoglucosan (delineated by color). Vertical dashed lines denote the boundaries of C^* bins where the number at the top of the bins indicate log C^* for each bin. Error bars show $\pm$ one standard deviation of 4 replicates of alkane standards. (B) Response factor for calibration compounds – n-alkanes, methoxyphenols (MPs), PAHs and levoglucosan (sugar) (delineated by color) as a function of the n-alkane equivalent eluting carbon number bin. The solid black line represents a degree 3 polynomial fitted to describe the variation in response factors of n-alkanes (equation: $y = 1.7 - 0.1x - 0.01x^2 + 0.0004x^3$) while the dotted black lines show the 95% confidence interval on the fit. The grey boxes in panel A are where the calibrated (labels on top of bin ranges) and estimated C^* overlap. Note: C^* vs. GC retention time data for saturated acids were collected fortuitously from another calibration exercise; a separate calibration for response factor was not completed and hence this data is missing from (B).

a sample medium along with an internal standard and analyzed by the TD/GC/MS. We fit a cubic function to describe the variation in response factor of n-alkanes vs. n-alkane bin (used as a proxy for GC retention time); fit parameters are given in Fig. 1 caption. Data across four calibration runs are included in this fit (error bars show standard deviation of replicates). The response factors for the n-alkanes calculated from these calibration experiments were consistent as indicated by the coefficient of variation (0.12 ± 0.08) calculated on the average response factors across the calibration experiments ($N = 4$). Response factors show a marked variation across the carbon number range, with average response factors for C_{10} to C_{19} and C_{31} to C_{40} n-alkanes 111% and 416% greater than those for C_{20} to C_{30} n-alkanes. The compounds in the methoxyphenol standard eluted in the same retention time intervals as C_{10}–C_{14} straight-chained alkanes and show a response factor larger than corresponding alkanes eluting in these bins by an average of $27\% \pm 18\%$. Levoglucosan also had a response factor 20% larger than the corresponding eluting n-alkane (C_{15}). In contrast, the PAHs elute later, across a larger range (C_{15}–C_{33} alkanes) and with a lower response factor compared to the alkanes by an average of $48\% \pm 8\%$. The confidence intervals on the n-alkane response factor fit generally included the response factors from the other calibration compounds explored here, suggesting that we can constrain the uncertainty introduced by varying response factors across compound classes.

3.2 Particulate matter emission factors

Fig. 2 demonstrates the diverse types of biomass burning (field, burnhut and RWC) studied by showing test-averaged $PM_{2.5}$ EF

(from integrated filter measurements) plotted against MCE. $PM_{2.5}$ EFs are inversely related with MCE across the different sources, as has been typically observed.[54,55] Amongst the sources

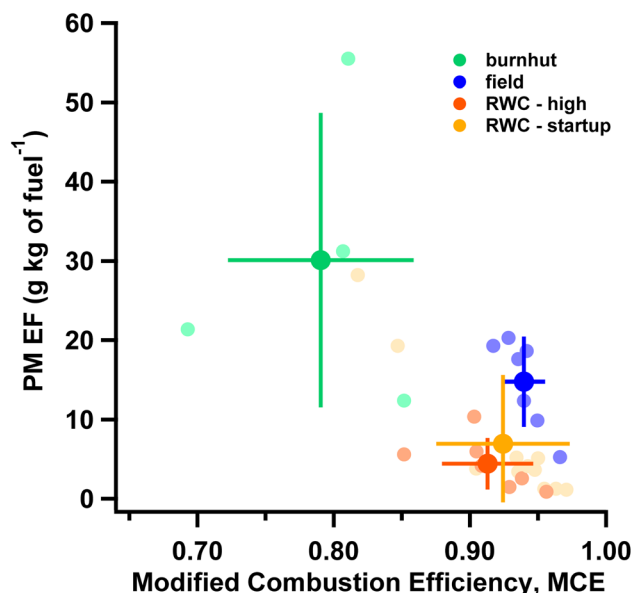**Fig. 2** $PM_{2.5}$ emission factors ($PM_{2.5}$ EF) as function of modified combustion efficiency (MCE) for different source emissions – burnhut, field, RWC phases (delineated by color). Faded markers represent test-averaged observations from individual integrated filter measurements while darker markers show the average $PM_{2.5}$ EF and MCE from an emissions source type with the error bars denoting the standard deviation across individual tests.

studied here, field burns had the highest average MCE (0.94 ± 0.02) while burn hut burns were the least efficient (MCE ~ 0.79), resulting in larger $PM_{2.5}$ EFs. An MCE threshold of 0.9 has often been used to demarcate smoldering *vs.* flaming combustion conditions[56] indicating burnhut combustion was primarily smoldering while the others were mostly flaming conditions. The RWC-high phase had the lowest average $PM_{2.5}$ EF (4.4 ± 3.3 g kg of fuel^{-1}). $PM_{2.5}$ EFs for field burns were consistent with other work where a range of 6.26 g kg of fuel^{-1} (crop residue) to 15.3 g kg of fuel^{-1} (boreal forest) was reported.[55] $PM_{2.5}$ EFs from RWC emissions overlapped with observations from literature where $PM_{2.5}$ EFs of 2.2 ± 1.2 g kg of fuel^{-1} was recorded across various fuels.[57] Fig. S3† shows OC and EC EFs plotted against MCE where OC EFs are inversely related to MCE (like $PM_{2.5}$ EFs) while EC EFs generally increase with MCE. PM and OC EFs from the combustion sources in this study span two orders of magnitude indicating diversity in emission characteristics. $PM_{2.5}$ mass is dominated by OC with OC/PM ratios of $54 \pm 16\%$, $63 \pm 9\%$ and $66 \pm 7\%$ for RWC, field and burn hut, respectively. EC/PM was significantly more variable and largest for RWC ($10 \pm 8\%$) and comparable for field and burnhut ($4 \pm 4\%$ and $2 \pm 2\%$ respectively). OM/OC ratios were estimated as: (PM EF−EC EF)/OC EF in the absence of more detailed chemical information (*e.g.* parameterization of aerosol mass spectra[58]). The average OM/OC ratio across all experiments was 1.53 ± 0.18 consistent with literature values;[59,60] this average was applied to OC EFs to infer OM EFs. The estimated OM EF + EC EF is plotted against $PM_{2.5}$ EF in Fig. S4.† In this study we emphasize the consistency in relationship between $PM_{2.5}$ and MCE across the different types of biomass burning and conditions rather than the absolute EF values. Fig. 2 shows that the samples included in this evaluation of the volatility distribution estimation method span a range of biomass burning emissions. However future work should systematically vary combustion and sampling parameters to explore sensitivities not explicitly considered here.

3.3 Volatility distribution profiles of biomass burning sources

Fig. 3A shows normalized volatility distributions (f_i) inferred from TD/GC/MS chromatograms of filter-in-tube biomass burning samples. The volatility distributions are presented as the mass fraction in log-spaced C^* bins applying the method described in Section 2.4. To compare the volatility distributions of different source emissions we group the bins into the three volatility ranges labeled on the plot: IVOC, SVOC and LVOC. IVOCs dominate the volatility distribution with average contributions of $75 \pm 9\%$, $80 \pm 6\%$, $84 \pm 15\%$ and $90 \pm 15\%$ of total organic emissions for burnhut, field, RWC – high and RWC – startup, respectively. The bins with log $C^* = 6$ dominate across the different combustion sources, with $50-80\%$ of total IVOC emissions contained in this bin. SVOCs represent $13 \pm 3\%$, $6 \pm 1\%$, $13 \pm 2\%$ and $8 \pm 1\%$ of total organic emissions for burnhut, field, RWC – high and RWC – startup, respectively. Finally, LVOCs contribute $12 \pm 4\%$, $14 \pm 9\%$, $3 \pm 2\%$ and $1 \pm 1\%$ for burn hut, field, RWC – high and RWC – startup, respectively.

The differences in contributions to LVOCs and SVOCs across the different combustion sources could play important differences in POA partitioning behavior. For example, a higher OA concentration will be required for RWC – high emissions to achieve the same particle mass fraction relative to field emissions because of higher SVOC and lower LVOC contributions, assuming that all other atmospheric conditions are the same.

Fig. S5† shows paired scatter plots of the mass fractions in each log C^* bin for the different source emissions to compare the distributions across burn types. Since the contribution in the log $C^* = 6$ bin is larger by more than a factor of 3 than the other bins, linear fits would be influenced by high leveraging. Instead, we calculate the root mean square error (RMSE) to the $1 : 1$ line to quantify deviations from complete agreement, indicated by an RMSE of 0, between two distributions and interpret the RMSEs in a relative manner. The RMSE was calculated in the vertical/horizontal direction, both giving the same result, as well as orthogonal to the $1 : 1$ line however only the latter is printed in Fig. S5† since the relative differences were the same across methods. According to this metric, the most similar distribution pairs were RWC high – RWC startup, field – RWC high and burn hut – field. In contrast, the burnhut – RWC startup comparison had the least similar distribution by this metric.

In Fig. 3B we show the volatility distributions as EFs by normalizing the mass emitted in each log C^* bin by the amount of fuel burnt as described in eqn (1). The bin mass emission factors span two orders of magnitude across the biomass burning combustion sources indicating variation consistent with PM emission factors discussed in Section 3.3. This indicates that fuel composition and combustion conditions influence contributions to log C^* bins and PM from integrated filter measurements.

3.4 Comparison of volatility distributions with literature

Fig. S6† shows comparisons of the volatility distributions shown in Fig. 3 with the distributions derived in May *et al.*[11] The measurement range in May *et al.*[11] spans log $C^* = -2$ to 4 bins and thus our distributions are re-normalized after removing the contributions from the log $C^* = 5$ and 6 bins to allow direct comparisons. Fig. S7† shows scatter plots of mass fractions in each log C^* bin from our source emissions and May *et al.*, with the largest differences arising from the bins: −2, 3 and 4. However, RMSEs calculated to the $1 : 1$ line were of similar magnitude across our various source distributions when compared to the May *et al.* distribution. Therefore, the variation within our different source type distributions is similar to that between ours and the May *et al.* distribution, and thus our distributions are similar to the May *et al.* distribution.

To explore the implications of differences in volatility distributions, Fig. 4A shows the particle mass fraction (X_p) predicted from the partitioning equation (eqn (1)) as a function of C_{OA}. We used the volatility distributions shown in Fig. S6† (normalized after removing log C^* bins 5 and 6) to derive these curves to enable comparison with partitioning behavior from May *et al.*[11]. Fig. S8† shows both the partitioning curves

© 2023 The Author(s). Published by the Royal Society of Chemistry

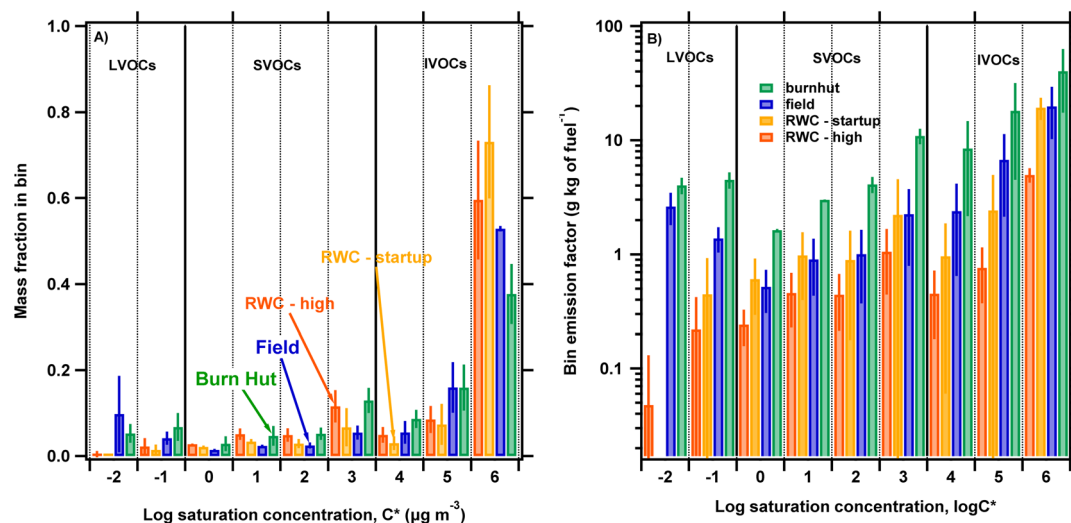*Environ. Sci.: Atmos.*, 2023, **3**, 11–23 | 17

Fig. 3 (A) Volatility distributions of biomass burning combustion sources (burnhut, field, RWC – high and RWC – startup; delineated by color) presented as mass fraction in each log-spaced saturation concentration (log C^*) bin. The mass fraction shown in each bin is the average bin mass from replicate ($N = 3$) samples while the error bars show the standard deviations of replicates. (B) Biomass burning source emission (delineated by color) volatility distributions presented as emission factors by normalizing the mass emitted in each log C^* bin by amount of fuel burnt. The bin emission factor showed in each bin is the average bin emission factor from replicate ($N = 3$) samples while the error bars show the standard deviations of replicates.

generated from these truncated volatility distributions and with those in Fig. 3A (including log C^* bins 5 and 6) for comparison, with the latter showing lower X_p values, especially at lower C_{OA}. Across the different source types, we observe maximum differences in predicted X_p at lower C_{OA}, with decreasing divergence

for increasing C_{OA}. This is due to the relatively larger differences in LVOC and SVOC contributions across the different source emissions. As the OA concentration increases, the differences in the contributions of lower and semi-volatile compounds matter less to POA partitioning as these bins are saturated. Between the
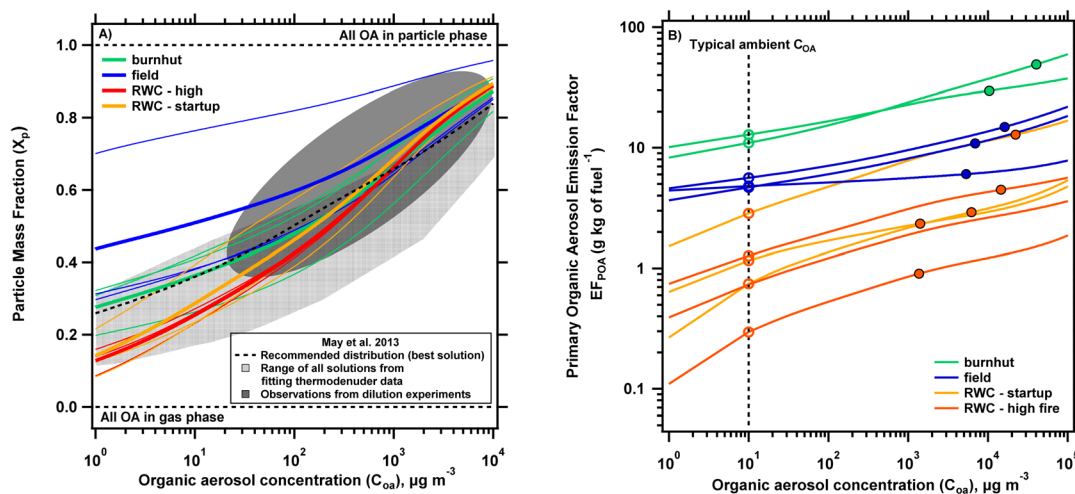

Fig. 4 (A) Partitioning plot showing the particle mass fraction (X_p) calculated using eqn (1) and volatility distributions shown in Fig. S6† (omitting logC* bins 5 and 6 and re-normalized to match observations from May *et al.* (2013a)) *vs.* organic aerosol concentration (C_{OA}). The biomass burning sources are delineated by color, with the thin lines showing the predicted partitioning from individual experiments and the thicker lines showing the average for each biomass burning type. Also plotted are observations from May *et al.* (2013a): (1) range of observations from chamber dilution experiments (dark gray oval), (2) predictions from the range of feasible solutions obtained from fitting thermodenuder data (light gray region), (3) predictions using their recommended biomass burning distribution (at 25 °C) (dotted black line). (B) Primary organic aerosol emission factor (POA EF) as a function of organic aerosol concentration (C_{OA}) derived using the partitioning equation and the volatility distributions shown in Fig. 3B (including all bins). The predicted partitioning for each replicate tube sample is shown with an individual line with each biomass burning type delineated by color. The closed circles indicate the POA EFs measured at the sampling concentration of each experiment while the open circles use the volatility distributions to predict POA EF at $C_{OA} = 10$ μg m^{-3} to represent an equivalent EF at dilute/ambient conditions.

18 | *Environ. Sci.: Atmos.*, 2023, **3**, 11–23

© 2023 The Author(s). Published by the Royal Society of Chemistry

RWC phases, the average predicted X_p for startup conditions is greater than that for high fire conditions by a maximum relative difference of 12.9% (at 5.8 µg m^{-3}), which decreases to <10% at 68 µg m^{-3} with increases in C_{OA} leading to further decreases in difference of X_p. This indicates that there are only minor differences in the predicted partitioning between the RWC phases. The difference in average predicted X_p is larger between burnhut and field burn conditions with a 40% difference at 10 µg m^{-3}, reducing to 24% at 100 µg m^{-3} and <10% at 790 µg m^{-3}. The greater differences here are mainly driven by larger X_p predictions from one replicate sorbent sample (relative to the other two) taken under field conditions. The difference in predicted X_p between burnhut and the other field samples (thin blue lines in a lower clustering in Fig. 4A) are <5% across all modeled C_{OA}. Thus, the X_p predicted for most samples collected from burnhut and field burn emissions are generally consistent, even though PM$_{2.5}$ EFs are >2 larger for burnhut compared to field emissions (Fig. 2). Finally, the difference in average predicted X_p between RWC – high and burnhut conditions is 43% at 10 µg m^{-3} and decreases to 13% at 100 µg m^{-3}. Overall, we see that the difference in X_p is about 10% (or lower) across the biomass burning sources at C_{OA} larger than 100 µg m^{-3} indicating relative similarity in volatility distributions and that partitioning is less sensitive to variations in distributions at higher concentrations.

Fig. 4A also plots gas–particle partitioning behavior from distributions developed by May *et al.* To compare predicted partitioning behavior from the current work, we consider three sets of results from this study: (1) observed partitioning from chamber dilution experiments; (2) predictions made from the range of feasible solutions obtained from fitting thermodenuder data; (3) predictions from the study's 'best overall' biomass burning distribution (at 25 °C). We see that our gas–particle partitioning profiles are generally well constrained within observations from dilution experiments (dark gray oval) and the range of statistically acceptable solutions from fitting thermodenuder data (light gray region) except for one field profile. The average burnhut profiles compared to the best solution profile from May *et al.* (dotted black line in Fig. 4A) shows a difference in predicted X_p of <5% throughout the modeled C_{OA} range, indicating close agreement in distributions from distinct methods but relatively consistent combustion methods (lab burns of diverse biomass types). Consistency in the predicted profiles from our study and May *et al.* support the viability of deriving volatility distributions by analyzing filter-in-tube sorbents using a TD/GC/MS for biomass burning emissions.

Fig. 4B shows partitioning plots in terms of POA emission factor as a function of C_{OA} using the volatility distributions presented in Fig. 3B along with the partitioning equation. Also shown are the POA EFs measured at OA sampling concentrations (which ranged between 1300 and 40 000 µg m^{-3}) represented by the closed markers. These concentrations are comparable to those in near-field fire plumes and much higher than typical ambient concentrations. The differences in combustion conditions and configurations (*e.g.* open *vs.* closed combustion) and fuel compositions result in POA emission

factor profiles spanning two orders of magnitude for the different biomass burning sources (POA EFs range from 0.9–49 g kg of fuel^{-1}). Based on the partitioning equation, smaller POA emission factors are expected at lower C_{OA} such as those found at ambient conditions. In Fig. 4B we show the estimated POA emission factor at 10 µg m^{-3} for individual test data using open markers. 10 µg m^{-3} is chosen as an arbitrary dilute/ambient concentration and was also used to model ambient scenarios in the analysis of Robinson *et al.* (2010). We acknowledge that ambient concentrations may be higher in fire impacted environments like those from woodstove emissions (tens of µg m^{-3}) and wildfire (tens or hundreds of µg m^{-3}) but choose this value for illustrative purposes. Predicted POA emission factors at 10 µg m^{-3} are 56−77%, 20−62% and 50−77% lower than POA emission factors measured at the sampling concentration for burnhut, field and RWC emissions respectively, demonstrating the dominant contribution of I/SVOCs on POA emissions. These ranges are a function of both volatility distributions and sampling conditions. If the volatility distributions are known, POA EFs can be estimated under any sampling conditions.

4. Implications, limitations, and future work

In this work, we quantified the contributions of S/I-VOCs from biomass burning sources with different combustion conditions and fuel types in the VBS framework. We measured both gas and particle phase concentrations of emitted organic aerosol by sampling on sorbent tubes inset with quartz filters, which allowed the observation of a larger range of volatility species ($-2 \leq \log C^* \leq 6$) than either sampling medium alone. This method was novel in its application for characterizing biomass burning emissions. We showed that, while there were notable differences in volatility distributions across burn types, the predicted partitioning using this method is consistent with previous observations from chamber dilution and thermodenuder experiments.[11] This agreement highlights the potential of predicting partitioning behavior of biomass burning emissions using filter-in-tube sorbent samples. The main advantages of using this method are: (1) the derived volatility distributions are more comprehensive since both gas and particle phase organics are measured together; (2) estimations can be made based on the analysis of a single sample using standard TD/GC/MS analytical instrumentation, and; (3) POA mass distributions can be constrained in the lowest volatility bins without the requirement of equilibrium with the gas phase during sampling. Gas–particle equilibrium is a requirement in dilution-based studies (which do not incorporate kinetic modeling) aimed at estimating volatility distributions and is challenging, especially at lower concentrations.[12] Further, this relatively simple sampling approach makes *in situ* measurements possible allowing future studies to characterize in-field measurements of the actual sources as opposed to relying on laboratory simulations.

An advantage of this approach is the potential to quantify emissions in higher C^* bins (log $C^* = 5, 6$), which may allow for

© 2023 The Author(s). Published by the Royal Society of Chemistry

Environ. Sci.: Atmos., 2023, **3**, 11–23 | 19

more accurate parameterizations of SOA formation potentials or gas–particle partitioning at very high sampling concentrations (100–1000 μg m^{-3}). The volatility distributions derivable from this method can also be useful for application in CTMs, the performance of which have previously benefitted from the addition of volatility information.[61–63] CTMs are important tools that can inform policy and regulations and thus, the addition of these distributions to model OA in CTMs can result in improved predictions relative to traditional approaches.

The volatility distributions derived for the biomass burning sources sampled here were generally consistent. IVOCs dominated the volatility distributions, accounting for 75–90% of the total contribution across the biomass burning sources, while SVOCs and LVOCs were responsible for 6–13% and 1–12%, respectively. Consistency in volatility distributions and predicted partitioning across the sources was observed despite PM emission factors spanning two orders of magnitude. However, substantial differences were also observed in the SVOC and LVOC contributions across the sources studied, which have implications on POA partitioning behavior. The influence on POA partitioning behavior is most pronounced at lower organic loadings. Although we did not perform molecular chemical speciation, the variability in composition from different types of biomass smoke has been observed previously.[64–66] Recent work has also shown the key influence of combustion temperature/ phase on VOC emission characteristics.[67] The partitioning behavior of biomass burning emissions is governed by thousands of semi-volatile species with varying chemical identities, vapor pressures and mixing properties. However, when considered together, the overall partitioning behavior of all these mixtures was similar enough to be represented using similar volatility distributions. In our analyses, we binned the TICs based on standard compound behavior. However, there is a potential to deconvolve the mass spectra further and extract more detailed chemical information. This chemical information can be used to inform yields for SOA production, with applications in air quality models or source apportionment. One of the key assumptions of this method is that compounds in the UCM behave like *n*-alkanes and have similar response factors. Analysis of calibration samples showed that polynomial fits describing response factors for a set of standard calibration compound classes were roughly constrained within the variation between different compounds. The resulting fit was best constrained between C_{15} and C_{30} while predicted response factors for later- and earlier-eluting compounds were more uncertain. However, combustion of biomass can also emit oxygenated IVOCs[68] which may not be measured by the TD/GC/ MS or remain in an unresolved state. The application of hydrocarbon response factors to these compounds may underestimate the mass in the IVOC bins as polar compounds tended to have lower response factors than hydrocarbons. Another key assumption involves correction of the organic mass estimated using thermal desorption gas chromatography mass spectrometry (TD/GC/MS) chromatograms with organic carbon (OC) filter measurements. The need for this correction factor likely arises because oxygenated compounds may not elute and thus are omitted from the UCM in chromatograms but are collected

on filter samples. Our correction assumes an even bias across the volatility range; this assumption cannot be tested with our methods but may be probed using more advanced gas chromatography methods. More complete speciation of organic compounds present in the gas and particle phase of combustion emissions is increasingly possible with the development of novel instrumentation and techniques.[39,68,69] Future work should derive POA volatility using these resources to validate these key assumptions in this method.

Conflicts of interest

There are no conflicts of interest to declare.

Acknowledgements

References

1 I. P. C. C., *The Physical Science Basis. Contribution of Working Group I to the Fifth Assessment Report of the Intergovernmental Panel on Climate Change*, Cambridge University Press, Cambridge, United Kingdom and New York, NY, USA, Geneva, Switzerland, 2014, p. 1535.

2 S. Fuzzi, U. Baltensperger, K. Carslaw, S. Decesari, H. Denier van der Gon, M. C. Facchini, D. Fowler, I. Koren, B. Langford, U. Lohmann, E. Nemitz, S. Pandis, I. Riipinen, Y. Rudich, M. Schaap, J. G. Slowik, D. V. Spracklen, E. Vignati, M. Wild, M. Williams and S. Gilardoni, Particulate matter, air quality and climate: lessons learned and future needs, *Atmospheric Chem. Phys.*, 2015, **15**, 8217–8299.

3 C. A. I. Pope, M. Ezzati and D. W. Dockery, Fine-Particulate Air Pollution and Life Expectancy in the United States, *N. Engl. J. Med.*, 2009, **360**, 376–386.

4 Health Effects Institute and State of Global Air, *A Special Report on Global Exposure to Air Pollution and its Disease Burden*, Boston, MA, 2019.

5 S. Chowdhury, S. Dey, S. Guttikunda, A. Pillarisetti, K. R. Smith and L. D. Girolamo, Indian annual ambient air quality standard is achievable by completely mitigating emissions from household sources, *Proc. Natl. Acad. Sci.*, 2019, **116**, 10711–10716.

6 L. Conibear, E. W. Butt, C. Knote, S. R. Arnold and D. V. Spracklen, Residential energy use emissions dominate health impacts from exposure to ambient particulate matter in India, *Nat. Commun.*, 2018, **9**, 617.

7   T. C. Bond, D. G. Streets, K. F. Yarber, S. M. Nelson, J. H. Woo and Z. Klimont, A technology-based global inventory of black and organic carbon emissions from combustion, *J. Geophys. Res. Atmospheres*, 2004, **109**, 1–43.

8   T. C. Bond, S. J. Doherty, D. W. Fahey, P. M. Forster, T. Berntsen, B. J. DeAngelo, M. G. Flanner, S. Ghan, B. Kärcher, D. Koch, S. Kinne, Y. Kondo, P. K. Quinn, M. C. Sarofim, M. G. Schultz, M. Schulz, C. Venkataraman, H. Zhang, S. Zhang, N. Bellouin, S. K. Guttikunda, P. K. Hopke, M. Z. Jacobson, J. W. Kaiser, Z. Klimont, U. Lohmann, J. P. Schwarz, D. Shindell, T. Storelvmo, S. G. Warren and C. S. Zender, Bounding the role of black carbon in the climate system: A scientific assessment, *J. Geophys. Res. Atmospheres*, 2013, **118**, 5380–5552.

9   C. Wiedinmyer, S. K. Akagi, R. J. Yokelson, L. K. Emmons, J. A. Al-Saadi, J. J. Orlando and A. J. Soja, The Fire INventory from NCAR (FINN): a high resolution global model to estimate the emissions from open burning, *Geosci. Model Dev.*, 2011, **4**, 625–641.

10 M. O. Andreae and D. Rosenfeld, Aerosol–cloud–precipitation interactions. Part 1. The nature and sources of cloud-active aerosols, *Earth-Sci. Rev.*, 2008, **89**, 13–41.

11 A. A. May, E. J. T. Levin, C. J. Hennigan, I. Riipinen, T. Lee, J. L. Collett, J. L. Jimenez, S. M. Kreidenweis and A. L. Robinson, Gas-particle partitioning of primary organic aerosol emissions: 3. Biomass burning, *J. Geophys. Res. Atmospheres*, 2013, **118**, 11327–11338.

12 A. P. Grieshop, J. M. Logue, N. M. Donahue and A. L. Robinson, Laboratory investigation of photochemical oxidation of organic aerosol from wood fires 1: measurement and simulation of organic aerosol evolution, *Atmospheric Chem. Phys.*, 2009, **9**, 1263–1277.

13 A. L. Robinson, N. M. Donahue, M. K. Shrivastava, E. A. Weitkamp, A. M. Sage, A. P. Grieshop, T. E. Lane, J. R. Pierce and S. N. Pandis, Rethinking Organic Aerosols: Semivolatile Emissions and Photochemical Aging, *Science*, 2007, **315**, 1259–1262.

14 M. K. Shrivastava, E. M. Lipsky, C. O. Stanier and A. L. Robinson, Modeling semivolatile organic aerosol mass emissions from combustion systems, *Environ. Sci. Technol.*, 2006, **40**, 2671–2677.

15 A. L. Robinson, A. P. Grieshop, N. M. Donahue and S. W. Hunt, Updating the Conceptual Model for Fine Particle Mass Emissions from Combustion Systems, *J. Air Waste Manag. Assoc.*, 2010, **60**, 1204–1222.

16 H. A. C. Denier van der Gon, R. Bergström, C. Fountoukis, C. Johansson, S. N. Pandis, D. Simpson and A. J. H. Visschedijk, Particulate emissions from residential wood combustion in Europe – revised estimates and an evaluation, *Atmospheric Chem. Phys.*, 2015, **15**, 6503–6519.

17 J. F. Pankow, An absorption model of gas/particle partitioning of organic compounds in the atmosphere, *Atmos Env*, 1994, **28**, 185.

18 N. M. Donahue, A. L. Robinson, C. O. Stanier and S. N. Pandis, Coupled partitioning, dilution, and chemical aging of semivolatile organics, *Env Sci Technol*, 2006, **40**, 2635–2643.

19 B. N. Murphy, N. M. Donahue, A. L. Robinson and S. N. Pandis, A naming convention for atmospheric organic aerosol, *Atmos. Chem. Phys.*, 2014, **14**(11), 5825–5839.

20 N. M. Donahue, J. H. Kroll, S. N. Pandis and A. L. Robinson, A two-dimensional volatility basis set – Part 2: Diagnostics of organic-aerosol evolution, *Atmospheric Chem. Phys.*, 2012, **12**, 615–634.

21 Y. Morino, S. Chatani, K. Tanabe, Y. Fujitani, T. Morikawa, K. Takahashi, K. Sato and S. Sugata, Contributions of Condensable Particulate Matter to Atmospheric Organic Aerosol over Japan, *Environ. Sci. Technol.*, 2018, **52**, 8456–8466.

22 Y. Zhao, C. J. Hennigan, A. A. May, D. S. Tkacik, J. A. de Gouw, J. B. Gilman, W. C. Kuster, A. Borbon and A. L. Robinson, Intermediate-volatility organic compounds: a large source of secondary organic aerosol, *Env Sci Technol*, 2014, **48**, 13743–13750.

23 J. J. Schauer, M. J. Kleeman, G. R. Cass and B. R. T. Simoneit, Measurement of Emissions from Air Pollution Sources. 2. C_1 through C_{30} Organic Compounds from Medium Duty Diesel Trucks, *Environ. Sci. Technol.*, 1999, **33**, 1578–1587.

24 J. J. Schauer, M. J. Kleeman, G. R. Cass and B. R. T. Simoneit, Measurement of Emissions from Air Pollution Sources. 3. C_1–C_{29} Organic Compounds from Fireplace Combustion of Wood, *Environ. Sci. Technol.*, 2001, **35**, 1716–1728.

25 C. J. Gaston, F. D. Lopez-Hilfiker, L. E. Whybrew, O. Hadley, F. McNair, H. Gao, D. A. Jaffe and J. A. Thornton, Online molecular characterization of fine particulate matter in Port Angeles, WA: Evidence for a major impact from residential wood smoke, *Atmos. Environ.*, 2016, **138**, 99–107.

26 M. D. Hays, C. D. Geron, K. J. Linna, N. D. Smith and J. J. Schauer, Speciation of Gas-Phase and Fine Particle Emissions from Burning of Foliar Fuels, *Environ. Sci. Technol.*, 2002, **36**, 2281–2295.

27 L. R. Mazzoleni, B. Zielinska and H. Moosmüller, Emissions of Levoglucosan, Methoxy Phenols, and Organic Acids from Prescribed Burns, Laboratory Combustion of Wildland Fuels, and Residential Wood Combustion, *Environ. Sci. Technol.*, 2007, **41**, 2115–2122.

28 A. A. May, A. A. Presto, C. J. Hennigan, N. T. Nguyen, T. D. Gordon and A. L. Robinson, Gas-particle partitioning of primary organic aerosol emissions: (1) Gasoline vehicle exhaust, *Atmos. Environ.*, 2013, **77**, 128–139.

29 X. Li, T. R. Dallmann, A. A. May, D. S. Tkacik, A. T. Lambe, J. T. Jayne, P. L. Croteau and A. A. Presto, Gas-Particle Partitioning of Vehicle Emitted Primary Organic Aerosol Measured in a Traffic Tunnel, *Env Sci Technol*, 2016, **50**(22), 12146–12155.

30 S. H. Jathar, N. Sharma, A. Galang, C. Vanderheyden, M. Takhar, A. W. H. Chan, J. R. Pierce and J. Volckens, Measuring and modeling the primary organic aerosol volatility from a modern non-road diesel engine, *Atmos. Environ.*, 2019, 117221.

31 A. P. Grieshop, M. A. Miracolo, N. M. Donahue and A. L. Robinson, Constraining the Volatility Distribution and Gas-Particle Partitioning of Combustion Aerosols

© 2023 The Author(s). Published by the Royal Society of Chemistry

Environ. Sci.: Atmos., 2023, **3**, 11–23 | 21

Using Isothermal Dilution and Thermodenuder Measurements, *Environ. Sci. Technol.*, 2009, **43**, 4750–4756.

32 I. Riipinen, J. R. Pierce, N. M. Donahue and S. N. Pandis, Equilibrium time scales of organic aerosol inside thermodenuders: Evaporation kinetics versus thermodynamics, *Atmos. Environ.*, 2010, **44**, 597–607.

33 R. Saleh, A. Shihadeh and A. Khlystov, On transport phenomena and equilibration time scales in thermodenuders, *Atmospheric Meas. Tech.*, 2011, **4**, 571–581.

34 P. K. Saha, A. Khlystov and A. P. Grieshop, Determining Aerosol Volatility Parameters Using a "Dual Thermodenuder" System: Application to Laboratory-Generated Organic Aerosols, *Aerosol Sci. Technol.*, 2015, **49**, 620–632.

35 Y. Fujitani, K. Sato, K. Tanabe, K. Takahashi, J. Hoshi, X. Wang, J. C. Chow and J. G. Watson, Volatility Distribution of Organic Compounds in Sewage Incineration Emissions, *Env. Sci Technol*, 2020, 11.

36 A. A. Presto, C. J. Hennigan, N. T. Nguyen and A. L. Robinson, Determination of Volatility Distributions of Primary Organic Aerosol Emissions from Internal Combustion Engines Using Thermal Desorption Gas Chromatography Mass Spectrometry, *Aerosol Sci. Technol.*, 2012, **46**, 1129–1139.

37 Y. Zhao, N. T. Nguyen, A. A. Presto, C. J. Hennigan, A. A. May and A. L. Robinson, Intermediate Volatility Organic Compound Emissions from On-Road Gasoline Vehicles and Small Off-Road Gasoline Engines, *Env. Sci. Technol.*, 2016, **50**, 4554–4563.

38 Y. Zhao, N. T. Nguyen, A. A. Presto, C. J. Hennigan, A. A. May and A. L. Robinson, Intermediate Volatility Organic Compound Emissions from On-Road Diesel Vehicles: Chemical Composition, Emission Factors, and Estimated Secondary Aerosol Production, *Env. Sci. Technol.*, 2015, **49**, 11516–11526.

39 D. R. Worton, G. Isaacman, D. R. Gentner, T. R. Dallmann, A. W. H. Chan, C. Ruehl, T. W. Kirchstetter, K. R. Wilson, R. A. Harley and A. H. Goldstein, Lubricating Oil Dominates Primary Organic Aerosol Emissions from Motor Vehicles, *Environ. Sci. Technol.*, 2014, **48**, 3698–3706.

40 J. Jiang, I. El-Haddad, S. Aksoyoglu, G. Stefenelli, A. Bertrand, N. Marchand, F. Canonaco, J.-E. Petit, O. Favez, S. Gilardoni, U. Baltensperger and A. S. H. Prévôt, *Influence of Biomass Burning Vapor Wall Loss Correction on Modelingorganic Aerosols in Europe by CAMx v6.50*, Atmospheric Sciences, 2020.

41 G. Ciarelli, I. El Haddad, E. Bruns, S. Aksoyoglu, O. Möhler, U. Baltensperger and A. S. H. Prévôt, Constraining a hybrid volatility basis-set model for aging of wood-burning emissions using smog chamber experiments: a box-model study based on the VBS scheme of the CAMx model (v5.40), *Geosci. Model Dev.*, 2017, **10**, 2303–2320.

42 G. Ciarelli, S. Aksoyoglu, I. El Haddad, E. A. Bruns, M. Crippa, L. Poulain, M. Äijälä, S. Carbone, E. Freney, C. O'Dowd, U. Baltensperger and A. S. H. Prévôt, Modelling winter organic aerosol at the European scale with CAMx: evaluation and source apportionment with a VBS parameterization based on novel wood burning smog chamber experiments, *Atmospheric Chem. Phys.*, 2017, **17**, 7653–7669.

43 C. D. Cappa and J. L. Jimenez, Quantitative estimates of the volatility of ambient organic aerosol, *Atmospheric Chem. Phys.*, 2010, **10**, 5409–5424.

44 L. E. Hatch, A. Rivas-Ubach, C. N. Jen, M. Lipton, A. H. Goldstein and K. C. Barsanti, Measurements of I/SVOCs in biomass-burning smoke using solid-phase extraction disks and two-dimensional gas chromatography, *Atmospheric Chem. Phys.*, 2018, **18**, 17801–17817.

45 J. Aurell, B. K. Gullett, C. Pressley, D. G. Tabor and R. D. Gribble, Aerostat-lofted instrument and sampling method for determination of emissions from open area sources, *Chemosphere*, 2011, **85**, 806–811.

46 X. Zhou, J. Aurell, W. Mitchell, D. Tabor and B. Gullett, A small, lightweight multipollutant sensor system for ground-mobile and aerial emission sampling from open area sources, *Atmos. Environ.*, 2017, **154**, 31–41.

47 B. Khan, M. D. Hays, C. Geron and J. Jetter, Differences in the OC/EC Ratios that Characterize Ambient and Source Aerosols due to Thermal-Optical Analysis, *Aerosol Sci. Technol.*, 2012, **46**, 127–137.

48 E. Grandesso, B. Gullett, A. Touati and D. Tabor, Effect of Moisture, Charge Size, and Chlorine Concentration on PCDD/F Emissions from Simulated Open Burning of Forest Biomass, *Environ. Sci. Technol.*, 2011, **45**, 3887–3894.

49 A. Holder, *Black Carbon Emissions From Residential Wood Combustion Appliances*, 2019, 76.

50 J. H. Kroll and J. H. Seinfeld, Chemistry of secondary organic aerosol: Formation and evolution of low-volatility organics in the atmosphere, *Atmos. Environ.*, 2008, **42**, 3593–3624.

51 J. F. Pankow and W. E. Asher, SIMPOL.1: a simple group contribution method for predicting vapor pressures and enthalpies of vaporization of multifunctional organic compounds, *Atmospheric Chem. Phys.*, 2008, **8**, 2773–2796.

52 R. Wathore, K. Mortimer and A. P. Grieshop, In-Use Emissions and Estimated Impacts of Traditional, Natural- and Forced-Draft Cookstoves in Rural Malawi, *Environ. Sci. Technol.*, 2017, **51**, 1929–1938.

53 G. Isaacman, D. R. Worton, N. M. Kreisberg, C. J. Hennigan, A. P. Teng, S. V. Hering, A. L. Robinson, N. M. Donahue and A. H. Goldstein, Understanding evolution of product composition and volatility distribution through in-situ GC × GC analysis: a case study of longifolene ozonolysis, *Atmospheric Chem. Phys.*, 2011, **11**, 5335–5346.

54 J. Jetter, Y. Zhao, K. R. Smith, B. Khan, T. Yelverton, P. DeCarlo and M. D. Hays, Pollutant Emissions and Energy Efficiency under Controlled Conditions for Household Biomass Cookstoves and Implications for Metrics Useful in Setting International Test Standards, *Environ. Sci. Technol.*, 2012, **46**, 10827–10834.

55 S. K. Akagi, R. J. Yokelson, C. Wiedinmyer, M. J. Alvarado, J. S. Reid, T. Karl, J. D. Crounse and P. O. Wennberg, Emission factors for open and domestic biomass burning for use in atmospheric models, *Atmospheric Chem. Phys.*, 2011, **11**, 4039–4072.

56 S. Collier, S. Zhou, T. B. Onasch, D. A. Jaffe, L. Kleinman, A. J. Sedlacek, N. L. Briggs, J. Hee, E. Fortner, J. E. Shilling, D. Worsnop, R. J. Yokelson, C. Parworth, X. Ge, J. Xu, Z. Butterfield, D. Chand, M. K. Dubey, M. S. Pekour, S. Springston and Q. Zhang, Regional Influence of Aerosol Emissions from Wildfires Driven by Combustion Efficiency: Insights from the BBOP Campaign, *Environ. Sci. Technol.*, 2016, **50**, 8613–8622.

57 S. Guofeng, W. Siye, W. Wen, Z. Yanyan, M. Yujia, W. Bin, W. Rong, L. Wei, S. Huizhong, H. Ye, Y. Yifeng, W. Wei, W. Xilong, W. Xuejun and T. Shu, Emission Factors, Size Distributions, and Emission Inventories of Carbonaceous Particulate Matter from Residential Wood Combustion in Rural China, *Environ. Sci. Technol.*, 2012, **46**, 4207–4214.

58 M. R. Canagaratna, J. L. Jimenez, J. H. Kroll, Q. Chen, S. H. Kessler, P. Massoli, L. Hildebrandt Ruiz, E. Fortner, L. R. Williams, K. R. Wilson, J. D. Surratt, N. M. Donahue, J. T. Jayne and D. R. Worsnop, Elemental ratio measurements of organic compounds using aerosol mass spectrometry: characterization, improved calibration, and implications, *Atmospheric Chem. Phys.*, 2015, **15**, 253–272.

59 E. J. T. Levin, G. R. McMeeking, C. M. Carrico, L. E. Mack, S. M. Kreidenweis, C. E. Wold, H. Moosmüller, W. P. Arnott, W. M. Hao, J. L. Collett and W. C. Malm, Biomass burning smoke aerosol properties measured during Fire Laboratory at Missoula Experiments (FLAME), *J. Geophys. Res.*, 2010, **115**, D18210.

60 J. S. Reid, R. Koppmann, T. F. Eck and D. P. Eleuterio, A review of biomass burning emissions part II: intensive physical properties of biomass burning particles, *Atmos. Chem. Phys.*, 2005, **5**(3), 799–825.

61 T. E. Lane, N. M. Donahue and S. N. Pandis, Simulating secondary organic aerosol formation using the volatility basis-set approach in a chemical transport model, *Atmos. Environ.*, 2008, **42**, 7439–7451.

62 Q. J. Zhang, M. Beekmann, F. Drewnick, F. Freutel, J. Schneider, M. Crippa, A. S. H. Prevot, U. Baltensperger, L. Poulain, A. Wiedensohler, J. Sciare, V. Gros, A. Borbon, A. Colomb, V. Michoud, J.-F. Doussin, H. A. C. Denier van der Gon, M. Haeffelin, J.-C. Dupont, G. Siour, H. Petetin, B. Bessagnet, S. N. Pandis, A. Hodzic, O. Sanchez, C. Honoré and O. Perrussel, Formation of organic aerosol in the Paris region during the MEGAPOLI summer campaign: evaluation of the volatility-basis-set approach within the CHIMERE model, *Atmospheric Chem. Phys.*, 2013, **13**, 5767–5790.

63 S. C. Farina, P. J. Adams and S. N. Pandis, Modeling global secondary organic aerosol formation and processing with the volatility basis set: Implications for anthropogenic secondary organic aerosol, *J. Geophys. Res.*, 2010, **115**, D09202.

64 G. R. McMeeking, S. M. Kreidenweis, S. Baker, C. M. Carrico, J. C. Chow, J. L. Collett, W. M. Hao, A. S. Holden, T. W. Kirchstetter, W. C. Malm, H. Moosmüller, A. P. Sullivan and W. Cyle, Emissions of trace gases and aerosols during the open combustion of biomass in the laboratory, *J. Geophys. Res. Atmospheres*, 2009, **114**, 1–20.

65 P. M. Fine, G. R. Cass and B. R. T. Simoneit, Chemical Characterization of Fine Particle Emissions from Fireplace Combustion of Woods Grown in the Northeastern United States, *Environ. Sci. Technol.*, 2001, **35**, 2665–2675.

66 P. M. Fine, G. R. Cass and B. R. Simoneit, Chemical characterization of fine particle emissions from the wood stove combustion of prevalent United States tree species, *Environ. Eng. Sci.*, 2004, **21**, 705–721.

67 K. Sekimoto, A. R. Koss, J. B. Gilman, V. Selimovic, M. M. Coggon, K. J. Zarzana, B. Yuan, B. M. Lerner, S. S. Brown, C. Warneke, R. J. Yokelson, J. M. Roberts and J. de Gouw, High- and low-temperature pyrolysis profiles describe volatile organic compound emissions from western US wildfire fuels, *Atmospheric Chem. Phys.*, 2018, **18**, 9263–9281.

68 D. R. Gentner, G. Isaacman, D. R. Worton, A. W. H. Chan, T. R. Dallmann, L. Davis, S. Liu, D. A. Day, L. M. Russell, K. R. Wilson, R. Weber, A. Guha, R. A. Harley and A. H. Goldstein, Elucidating secondary organic aerosol from diesel and gasoline vehicles through detailed characterization of organic carbon emissions, *Proc. Natl. Acad. Sci.*, 2012, **109**, 18318–18323.

69 A. R. Koss, K. Sekimoto, J. B. Gilman, V. Selimovic, M. M. Coggon, K. J. Zarzana, B. Yuan, B. M. Lerner, S. S. Brown, J. L. Jimenez, J. Krechmer, J. M. Roberts, C. Warneke, R. J. Yokelson and J. de Gouw, Non-methane organic gas emissions from biomass burning: identification, quantification, and emission factors from PTR-ToF during the FIREX 2016 laboratory experiment, *Atmos. Chem. Phys.*, 2018, **18**, 3299–3319.

© 2023 The Author(s). Published by the Royal Society of Chemistry

Environ. Sci.: Atmos., 2023, **3**, 11–23 | **23**